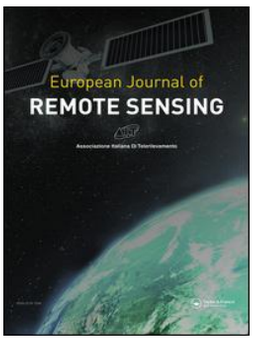

European Journal of Remote Sensing

ISSN: (Print) 2279-7254 (Online) Journal homepage: http://www.tandfonline.com/loi/tejr20

The role of both location and radiometer accuracy on the SSI performance in discriminating the atmospheric conditions

Ada Vittoria Bosisio, Ermanno Fionda, Piero Ciotti & Antonio Martellucci

To cite this article: Ada Vittoria Bosisio, Ermanno Fionda, Piero Ciotti & Antonio Martellucci (2014) The role of both location and radiometer accuracy on the SSI performance in discriminating the atmospheric conditions, European Journal of Remote Sensing, 47:1, 671-684, DOI: 10.5721/EuJRS20144738

To link to this article: https://doi.org/10.5721/EuJRS20144738

Published online: 17 Feb 2017.

European Journal of Remote Sensing - 2014, 47: 671-684
doi: 10.5721/EuJRS20144738
Received 28/02/2013, accepted 02/09/2014

European Journal of Remote Sensing
An official journal of the Italian Society of Remote Sensing

www.aitjournal.com

The role of both location and radiometer accuracy on the SSI performance in discriminating the atmospheric conditions

Ada Vittoria Bosisio[1]*, Ermanno Fionda[2], Piero Ciotti[3] and Antonio Martellucci[4]

[1]CNR\IEIIT c/o Politecnico di Milano, Milano, Italy
[2]Fondazione Ugo Bordoni (FUB), Roma,Italy
[3]Dept. of Industrial, Information Engineering and Economics, University of L'Aquila, L'Aquila, Italy
[4]ESA-ESTEC, TEC-EEP, Noordwijk, Nederland
*Corresponding author, e-mail address: adavittoria.bosisio@ieiit.cnr.it

Abstract
This study addresses the sensitivity of the Sky Status Indicator (SSI) with respect to both the radiometer accuracy and location of three stations included in the ground segment of the Alphasat experiment. The SSI aims at detecting the atmospheric conditions along a slant path, exploiting radiometric data at 20/30 GHz. The analysis is performed on synthetic brightness temperatures computed from a database of radiosonde profiles collected in De Bilt (NL), Milano (I), and Roma (I) through forward modelling. The SSI sensitivity to both radiometric resolution and bias error is computed for elevation angles equal to 27.6, 35.5, 40.2, 69.6, and 90°. Robustness of SSI boundary threshold values between clear and cloudy sky conditions is assessed.
Keywords: Atmospheric propagation, microwave radiometry, satellite communication.

Introduction
The discrimination of sky propagation conditions is relevant for a variety of applications in atmospheric sciences, such as microwave remote sensing and satellite communications. Furthermore, deep space applications can benefit from a tool indicating clear sky conditions for the estimate of the tropospheric path delay (emission/absorption processes only due to gaseous constituents) [Keihm and Marsh, 1996; Tanner and Riley, 2003; Basili et al., 2014], whereas the information on the absence of rain events is valuable for the community interested in the water vapour and cloud liquid retrieval [Westwater, 1978; Elgered et al., 1982; Hogg et al., 1983, Westwater et al., 1990]. In addition to that, the real time knowledge of occurring rain events, in a volume of an operative beacon, can support the adoption of Fade Mitigation Techniques (FMT) to overcome the degradation of the signal quality [Gataullin, 2009; De Montera et al., 2010].
In this context, ground-based microwave radiometers (MWR) are exploited for their ability to sense the atmospheric thermodynamic features of a satellite channel [Tanner and Riley, 2003; Ware at al., 2003; Crewell et al., 2009]. Based on brightness temperature values $T_b(f)$,

measured by a MWR at 20/30 GHz band, the authors developed a scalar indicator, the Sky Status Indicator (SSI), that can help in discriminating among clear, cloudy and rainy sky conditions [Bosisio and Capsoni, 1995; Bosisio et al., 2012]. A dataset of $T_b(f)$ values, collected in Cabauw (NL) by the ESA ATPROP System [Rose, 2008] along zenithal (θ=90°) and slant path (at θ=69.6°), was used to compute the SSI as the ratio of $T_b(f)$ values at 31.4 and 23.8 GHz, properly modified to subtract the contribution of the gaseous dry emission (mainly due to O_2) of the Earth atmosphere [Bosisio et al., 2012]. Afterwards, the SSI discrimination capabilities were assessed against rain gauge precipitation measurements demonstrating the good performances of the proposed indicator to discriminate the three above mentioned sky propagation conditions [Bosisio et al., 2013a, 2013b].

On the bases of its definition, the SSI depends on the atmospheric dry contribution and it is necessary to take into account this features according to the site location and to the pointing angle of the radiometric antenna.

This paper focuses on the SSI sensitivity with respect to a set of elevation angles and site locations involved in the incoming European Alphasat "Aldo Paraboni" (TDP 5) communication experiment at the Q/V band [Alphasat Project - http://telecom.esa.int/telecom/www/object/index.cfm?fobjectid=1138; Marzano et al., 2012; Ruggieri et al., 2012]. Alphabus was launched into its planned orbit on July 25th 2013, and it reached its GEO position (25° East) on October 8th 2013. The sensitivity analysis was performed only under non-rainy conditions, at five possible operational elevation angles (at 27.6, 35.5, 40.2, 69.6 and 90°) and three sites: De Bilt (NL), Milano (I), and Roma (I). These latter are candidate to be among the nodes of the European Alphasat ground-segment.

Specifically, all the analysis discussed hereafter are based on simulated $T_b(f)$ values computed by using a radiative transfer forward model (MPM91) [Liebe et al., 1991] also including a microphysical-consistent non-precipitating 2D cloud structure model [Salonen and Uppala, 1991; Mattioli et al., 2009], applied to each radiosonde profile (RAOB) collected during 2002-2008 in the selected sites.

As a result of the study, the coefficient for the computation of SSI is expressed as a linear function of the air mass (mean elevation angles), for each of the selected sites.

Moreover, focusing on the meaning of the SSI, the major concern is related to the reliability of the two SSI boundary threshold values: the first one between clear and cloudy sky (SSI_{CC}), and the second between cloudy and rainy sky conditions (SSI_{CR}). The discrimination capability of SSI_{CR} is of interest for the onset of whichever strategy to contrast microwave link impairments mainly caused by rain events.

The discrimination capability of SSI_{CC} can be used to assess a "reference level" for the atmospheric attenuation, experienced under clear sky conditions, towards the beacon level calibration through a *bias removal* procedure. This latter technique developed and applied during previous European propagation experiment (OPEX: Olympus Propagation EXperiment) [OPEX, 1994] should be reused in the Alphasat experiment.

A robustness analysis focuses on the SSI_{CC} boundary value to assess the impact on its discrimination capabilities of both: a) the radiometric instrumental resolution, adding a white Gaussian noise to $T_b(f)$ values; b) the radiometric calibration errors (through a bias of 1-4 K). The un-calibrated operational periods can seriously affect $T_b(f)$ measurements, mainly in case of low emission levels as under clear sky conditions.

In addition, some preliminary results on the strategy to set SSI_{CC} value according to the

probability of false negative that one can accept for the case under study are included. Similar analysis can be done on the SSI_{CR}, but unfortunately reliable and appropriate datasets of simulations under rainy sky conditions are not available at this stage.

Sky Status Indicator (SSI)

The SSI basic assumption is that the ratio of concurrent ground-based $T_b(f)$ in the 20/30 GHz band depends on the thermodynamic state of the atmosphere. Consequently, the SSI has the following definition [Bosisio et al., 2012, 2013b]:

$$SSI = \frac{\tilde{T}_{31}}{T_{23}} \quad [1]$$

where T_{23} stands for the T_b at 23.8 GHz, $\tilde{T}_{31} = \tilde{T}_b(31)$ is a modified T_b at 31.4 GHz according to:

$$\tilde{T}_{31} = T_{31} - c_0 \quad [2]$$

In [2] the coefficient c_0 depends on both location and elevation angle. Numerically, the c_0 is the intercepts of a linear best fit performed on simulated subset couples of (T_{23}, T_{31}) strictly referred to clear sky conditions. From a radiative point of view, the c_0 accounts for only the atmospheric dry contribution along the observed path. The following section focuses on the c_0 assessment as a function of elevation angles at each selected site.

Clear sky analysis: c_0 dependence on elevation and location

This analysis aims at assessing the dependence of the c_0 coefficient [2] on both the elevation angle and the site location to single out a more general SSI formulation. To this purpose a RAOB dataset (see Tab. 1) was employed to compute simulated $T_b(f)$ values through the MPM91 using the Rosenkranz model [Rosenkranz, 1999] to calculate the gaseous absorptions, and the modified Salonen model [Salonen and Uppala, 1991] for the non precipitating cloud contributions [Mattioli et al., 2009].

Thanks to a proper set of retrieval coefficients, the integrated water vapour (IWV) and the non precipitating cloud liquid path (LWP) were computed from simulated $T_b(f)$ values, associated with each RAOB profile for the three sites [Fionda et al., 2008]. RAOB profiles showing a LWP ≤ 0.001 mm were classified as in clear sky conditions as well as the associated $T_b(f)$ values forming the requested subset on which to compute the coefficient c_0 [2]. Table 1 reports the percentage of the classified clear sky RAOB profiles for each selected site.

Table 1 - RAOB database: geographic parameters and RAOB profile features.

Site	Period	Lat(°), Long(°)	Altitude a.s.l. [m]	RAOBs Samples	RAOBs Clear sky (%)	RAOBs Cloudy sky (%)
De Bilt (NL)	2002-2008	52.10 N, 5.18 E	4	3618	42	58
Milano (I)	2002-2008	45.43 N, 9.28 E	109	6158	55	45
Roma (I)	2002-2008	41.65 N, 12.48 E	70	5984	65	35

Figure 1 shows the c_0 values as a function of the air mass computed for De Bilt, Milano and Roma at the chosen set of elevation angles (27.6, 35.5, 40.2, 69.6 and 90°) together with the linear regression behaviours. For each location (denoted by the subscript l) it turns out that the c_0 coefficient has the following dependence with the elevation angle/air mass:

$$c_0 = a_l + b_l \cdot airmass \quad [3]$$

where the a_l and b_l values are reported in Table 2. The parameters (a_l and b_l) show a variability of about 15% and 7%, respectively, which can account for the joint effects of the site's climatological region and geographic features.

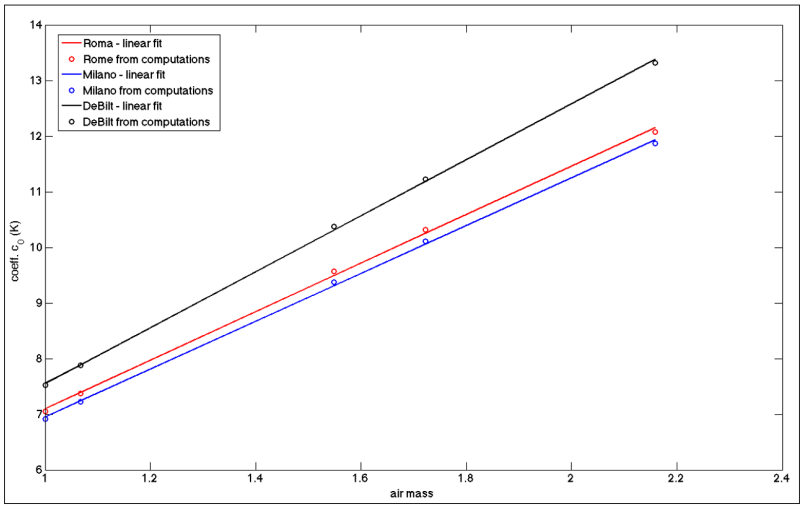

Figure 1 - The coefficients c_0 and the linear regression behaviours w.r.t. air mass values for the three locations.

Table 2 - The parameter values in [3] to compute the c_0 coefficient.

Site	a_l	b_l
De Bilt (NL)	2.53	5.02
Milano (I)	2.65	4.30
Roma (I)	2.74	4.36

Figure 2 shows the SSI averaged values derived from the three synthetic clear sky conditions $T_b(f)$ subsets (red dots) with respect to the chosen set of air masses /elevation angles at each site. The error bars indicate the interval of ±1 standard deviation (S.D.) about the average value. S.D. is equal to about 3.7%, 4.3%, and 4% of the average value for De Bilt, Milano and Roma, respectively. A regression analysis performed on the average values evidenced the linear relationship between the SSI values and the air mass ones:

$$SSI_l = s_{1l} + s_{2l} \cdot airmass \quad [4]$$

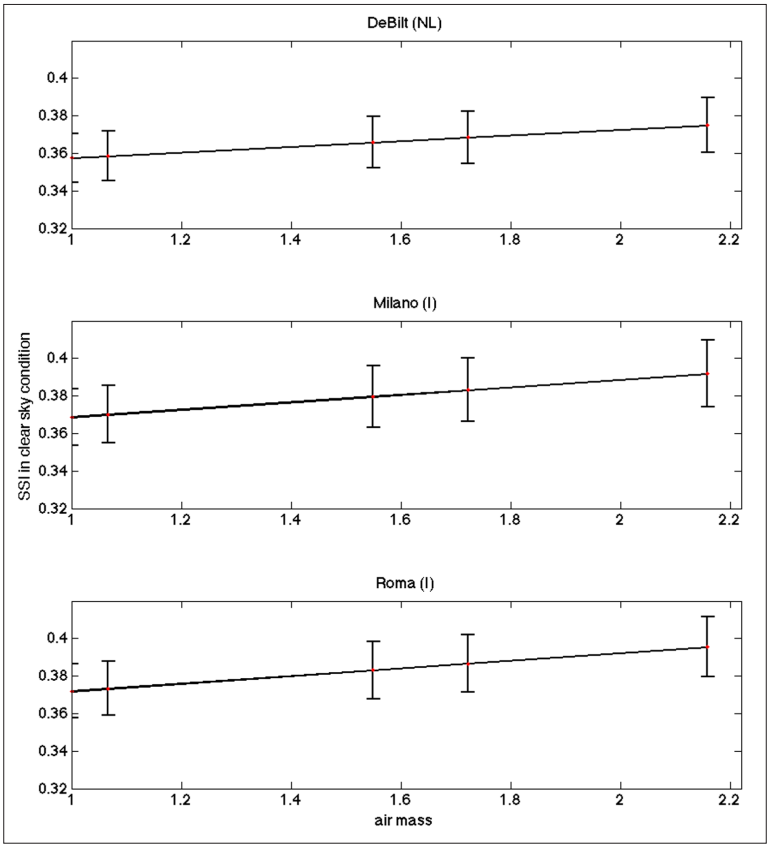

Figure 2 - The average SSI (red dots) with the associated standard deviation values (bars) versus the elevation angle/air mass, for the three selected sites. The solid lines represent the linear regression best fit. The SSI values are strictly associated to the clear sky conditions.

In [4] the subscript *l* refers to the specific site; the s_{1l} and s_{2l} coefficient values are reported in Table 3.

Table 3 - SSI coefficients with respect to elevation angle/air mass formulation according to [4].

Site	s_{1l}	s_{2l}
De Bilt (NL)	0.3425	0.0151
Milano (I)	0.3487	0.0200
Roma (I)	0.3516	0.0204

The slight variability of the angular coefficient (s_{2l}) should be due to features of the site's climatological region. The SSI intercepts value (s_{1l} at air mass=1) represents the total dry atmospheric contribution. The air mass dependence in the SSI values can be removed subtracting the corresponding values due to [4], as evidenced in Figure 3. After that, the

SSI amplitude shows an intrinsic variability of ± 0.06 in Milano and Rome sites and of ± 0.04 in De Bilt, corresponding to approximately at the 15% of the average SSI value.

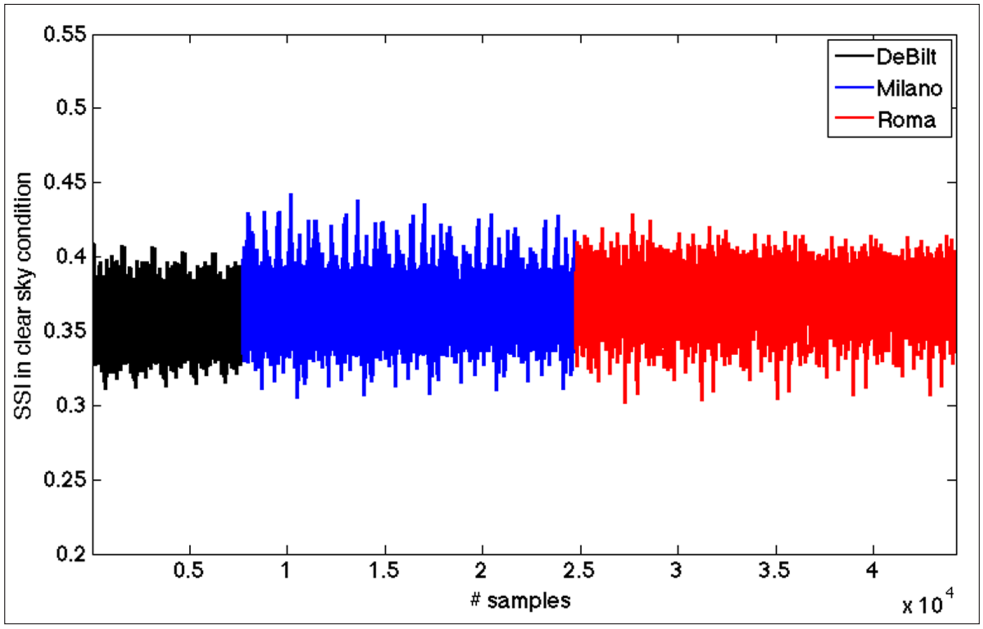

Figure 3 - All computed SSI values under clear sky conditions, after air mass effects removal.

Computation of the boundary threshold value SSI_{CC}

SSI and its boundary threshold values were set on measured $T_b(f)$ with the aim of using them as flags to discriminate sky propagation conditions in real time computation [Bosisio et al., 2013a, 2013b]. In particular, the SSI_{CC} boundary threshold value aims at discriminating the atmospheric propagation conditions between clear and cloudy sky conditions. The discussed investigation is based on simulated $T_b(f)$ data, without any additive rainy effects. In order to validate the reliability in identifying clear sky events, it is needed to test the SSI_{CC} robustness with respect to noisy measurements, and / or errors in the calibration procedure of the radiometer.

The SSI_{CC} boundary threshold value is singled out as the one at which the probability density function (PDF) of SSI computed on the $T_b(f)$ simulated under clear sky conditions equals the PDF of SSI for the $T_b(f)$ simulated in cloudy sky conditions, as shown in the top panel of Figure 4, where the SSI_{CC} value computed for De Bilt at 90° is highlighted. For completeness, the bottom panel of Figure 4 reports separately the histogram of the SSI relative to $T_b(f)$ simulated under clear sky conditions (leftmost image) and of the SSI relative to $T_b(f)$ simulated in cloudy sky conditions (rightmost image).

The SSI_{CC} values were computed for each site and elevation angle, after normalization of the two PDFs, i.e. the ones relative to clear sky and cloudy sky conditions, to the overall time duration (# of samples) of the dataset to which they are referred. These values, indicated as data without noise, are reported, for each site, in Table 4.

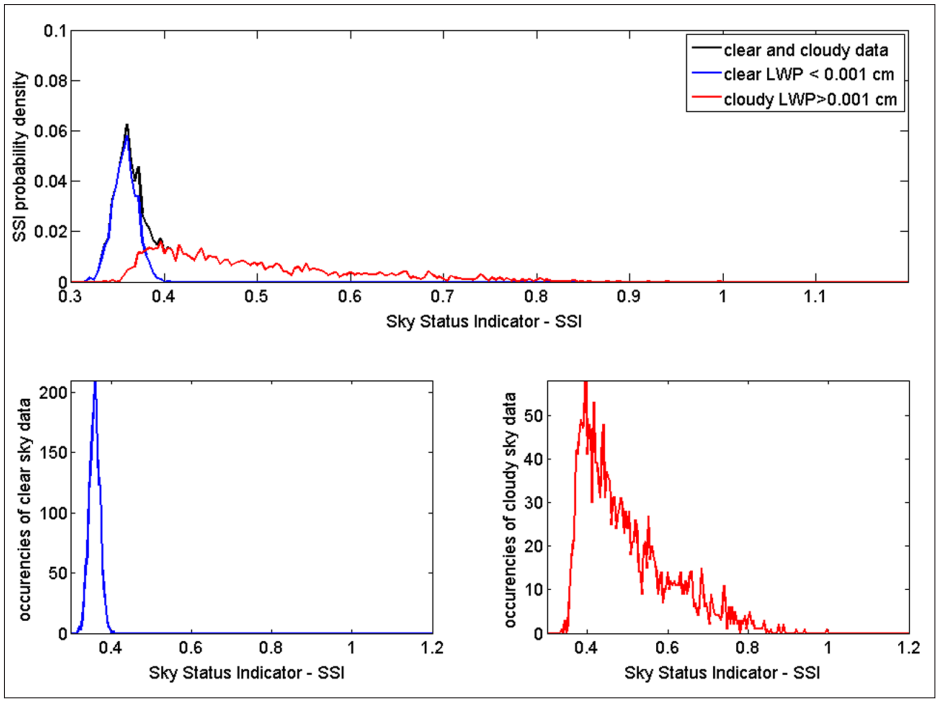

Figure 4 - De Bilt PDF (top panel) and histograms (bottom panel) of SSI computed in clear (blue) and cloudy (red) sky conditions. All data refer to the zenith. The black line refers to the whole dataset.

Table 4 - The boundary threshold average values of SSI_{CC} computed on the outcome of the RTE forward solution: using $T_b(f)$, without noise, and the perturbed $T_{bn}(f)$, with noise.

El. Ang. (°) /Air mass	De Bilt (NL)		Milano (I)		Roma (I)	
	$<SSI_{CC}>$					
	without noise	with noise	without noise	with noisy	without noise	with noise
27.6/2.158	0.400	0.394	0.418	0.420	0.424	0.426
35.5/1.722	0.390	0.390	0.410	0.412	0.416	0.416
40.2/1.549	0.388	0.388	0.406	0.410	0.412	0.410
69.6/1.067	0.380	0.386	0.396	0.400	0.402	0.404
90/1	0.380	0.382	0.394	0.396	0.400	0.402

Measurement accuracy and improper calibration effects on SSI_{CC}

The impact of the $T_b(f)$ measurements accuracy and improper calibration on SSI_{CC} values is treated in two separate steps. Firstly, the simulated $T_b(f)$ were corrupted with an additive white Gaussian noise (AWGN) with standard deviation (σ) equal to 0.25 K to account for the limited radiometric resolution. Afterwards, a bias of ±1 and ±4 K was added to reproduce measurements under improper calibration periods. The boundary threshold values were computed as for the data without noise but on 500 noisy iterations. Then, for each configuration, i.e. site and elevation angle and noise contribution, the SSI was computed from perturbed noisy temperatures as:

$$T_{bn}(f) = T_b(f) + N(0,\sigma^2) \qquad \sigma = 0.25K \qquad [5]$$
$$T_{bnp}(f) = T_{bn}(f) \pm i \qquad i = 1,2\ K$$

where $T_{bn}(f)$ is the noisy realization of $T_b(f)$, through the addition of the AWGN function $N(0, \sigma^2)$, and $T_{bnp}(f)$ accounts for the non calibrated noisy brightness temperature.
Table 4 reports the average boundary threshold values, $<SSI_{CC}>$ noisy data, computed by using $T_{bn}(f)$ for the three sites and all the elevation angles. Remarkably, the difference between the SSI_{CC} values computed from data without noise and the noisy $<SSI_{CC}>$ ones is about 1%. As a conclusion, SSI proved its robustness against random errors that can affect measurements.
The $<SSI_{CC}>$ noisy values computed by using $T_{bnp}(f)$ are shown in the bar plots of Figures 5-7, according to air mass values and for each site.

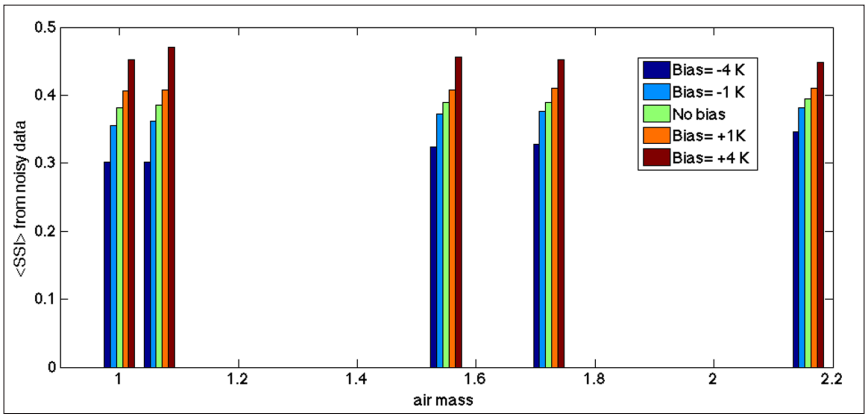

Figure 5 - Results of improper calibration effects (De Bilt): SSI_{CC} average value from perturbed $T_{bnp}(f)$ as in [5].

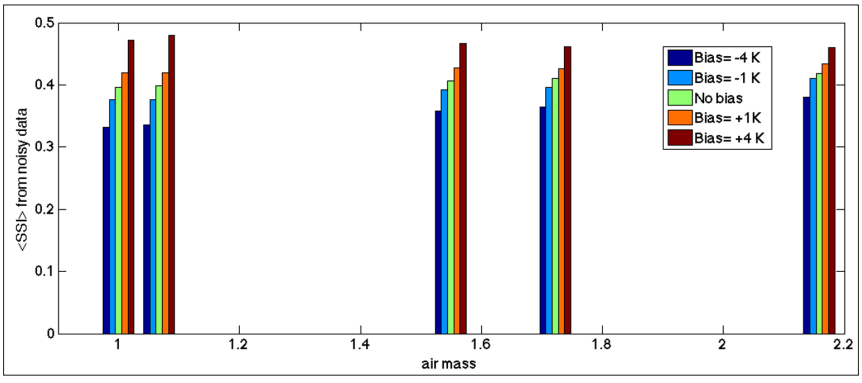

Figure 6 - Results of improper calibration effects (Milano): SSI_{CC} average value from perturbed $T_{bnp}(f)$ as in [5].

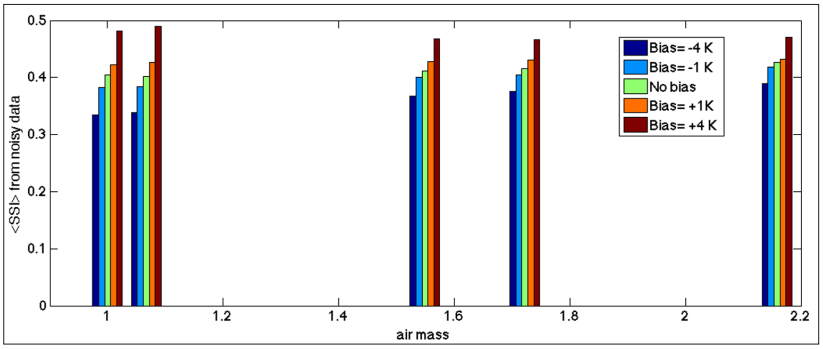

Figure 7 - Results of improper calibration effects (Roma): SSI_{CC} average value from perturbed $T_{bnp}(f)$ as in [5].

As far as the effects of the bias are concerned, the smallest variation occurs in Roma at θ=27.4° and it is about ±2% and -8/+10% - corresponding to ±1 and ±4 K, respectively - of the estimated average value of SSI_{CC} without bias, $<SSI_{CC}>$.
The greatest variation w.r.t $<SSI_{CC}>$ is observed for the De Bilt site along the zenithal path, with a difference of about ±6% and -18/+25 %, with a bias of ±1 and ±4 K, respectively. It is not surprising that along the zenithal path, corresponding to the lowest air mass and brightness temperatures in clear sky conditions, a bias gives raise to great variation in the SSI and, conversely, that at the lowest elevation angle, corresponding to the highest air mass and brightness temperatures in clear sky, a bias up to 4 K gives raise to the smallest variations in the average SSI values. The observed maximum and minimum variations are in agreement with the SSI values issued from the forward model computations as in De Bilt and in Roma they assume the lowest and the greatest values at the two specified elevation angles (see Tab. 4).

Performance analysis of SSI_{CC} discrimination capabilities

The SSI_{CC} boundary threshold average values reported in Table 4 were used to identify atmospheric clear or cloudy sky conditions associated to each RAOB profile that generates synthetic $T_b(f)$ values. The analysis was performed considering $T_{bn}(f)$. Table 5 reports the percentages of cloudy RAOB profiles identified by both SSI_{CC} boundary threshold values reported in Table 4 for each site. Furthermore, Table 5 reports the percentage of RAOB profiles identified as under cloudy sky conditions by the LWP content (Tab. 1).

Table 5 - Percentage of cloudy RAOB profiles identified by using SSI_{CC} criterion and the percentage of RAOBs profiles, at zenith (last line boldface), identified by the LWP criterion.

El. Ang. (°) /Air mass	De Bilt (NL)		Milano (I)		Roma (I)	
	$<SSI_{CC}>$					
	(%)	with noise (%)	(%)	with noise (%)	(%)	with noise (%)
27.6/2.158	53.9	57.5	42.0	40.0	29.9	28.4
35.5/1.722	55.5	57.4	40.9	41.2	28.9	30.1
40.2/1.549	55.1	57.6	40.9	40.4	28.9	32.5
69.6/1.067	55.1	52.7	40.0	39.4	28.4	28.7
90/1	54.4	54.3	40.0	40.0	28.8	28.5
	58		**45**		**35**	

Focusing on the De Bilt site at the zenith view, the validation of the discrimination capability based on the SSI_{CC} boundary thresholds (Tab. 4) underestimates of about 3% with respect to the results given by the LWP criterion. This discrepancy is justified by the fact that the threshold filtering introduces some false cases. The number of RAOB profiles classified under cloudy sky conditions by the LWP criterion is 2080 over 3618 (~ 58 %), in view of 1970 profiles (~ 54.5 %) due to the SSI_{CC} boundary threshold. Continuing to refer to De Bilt, Figure 8 (that highlights the top panel of Fig. 4) shows two PDF areas, the blue one corresponding to false cloudy RAOB profiles (69 profiles) and the red one corresponding to false clear RAOB sky profiles (179 profiles), adopting the SSI_{CC} criterion (SSI_{CC} boundary threshold=0.38).

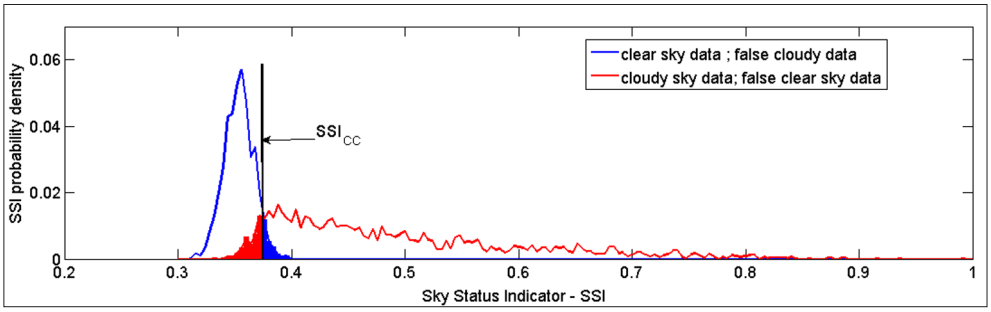

Figure 8 - De Bilt PDF (from Fig. 4): clear and cloudy sky condition false detection.

Table 6 reports the percentage of false identified cases for each elevation angle and site location. These results are obtained by using the noise-free $<SSI_{CC}>$ values.

Table 6 - Classification results: false identified clear sky and false identified cloudy sky by using noise-free $<SSI_{CC}>$ threshold criterion.

El. Ang. (°) / air mass	De Bilt (NL)		Milano (I)		Roma (I)	
	false identified cloudy data (%)	false identified clear data (%)	false identified cloudy data (%)	false identified clear data (%)	false identified cloudy data (%)	false identified clear data (%)
27.6/2.158	2.2	22.8	8.1	17.1	5.4	15.7
35.5/1.722	2.7	17.2	6.5	15,7	3.8	14.4
40.2/1.549	2.7	16.8	6.2	14.6	3.7	13.5
69.6/1.067	3.8	11.14	5.5	11.9	2.9	10.5
90/1	3.5	10.9	6	11.2	3.1	9.8

With the exception of the false identified cloudy data in De Bilt, all percentage values increase with decreasing elevation. This behaviour is related to the length of the observed path. The longer and wider the antenna volume, the more the non-homogeneity of the atmosphere near the ground can introduce ambiguity in the status detection based on the ratio between brightness temperature values.

The role of the boundary threshold criterion in discriminating between cloudy and clear sky conditions is shown in Figure 9, where the scatter plot of $T_b(31.4)$ versus $T_b(23.8)$ computed

for De Bilt at the zenith is displayed. The false identified cloudy data and clear sky data are coloured in cyan and magenta, respectively. All these points are placed along the line that limits the two sky status regions.

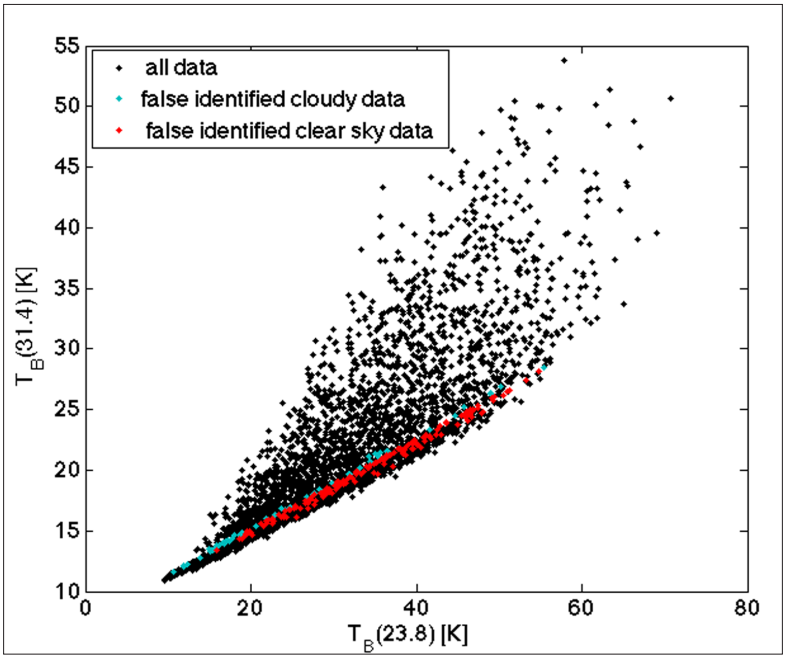

Figure 9 - Scatter plot of simulated T_b(31.4) versus T_b(23.8) for De Bilt at the zenith.

The underestimation of the number of cloudy scenarios adopting the SSI_{CC} boundary criterion derives from the tail of the PDF curve that is cut by the threshold line. This fact suggests the setting of a threshold boundary value different from the proposed one, according to other requirements, as for example the accepted rate of failure in the identification process. In other words, the boundary threshold value can be set following the Neyman-Pearson optimal detector approach [Neyman and Pearson, 1933]. Therefore, the threshold can be chosen differently whether one needs to detect the clear sky condition occurrences or alternatively would be sure to be in presence of cloudy conditions [Bosisio et al., 2014].
The percentage of false identified cases changes with the $<SSI_{CC}>$ value. For De Bilt (θ=90°) case, if one wishes to discriminate the cloud presence along the observed path it would be preferable to choose $<SSI_{CC}> = 0.388$, which occurs at the maximum of the PDF under cloudy conditions (red line in Fig. 4), obtaining as a result the proper detection of the 86 % of cloudy condition cases with a probability of false cloudy condition detection equal to 0.8 %. This threshold value detects properly the 99.2 % of clear sky condition, including a 14 % of false clear sky detected.
As a conclusion, given a historical dataset of occurrences, the boundary threshold value can be chosen according to the scope of interest in the location under test.

Conclusions

The scalar indicator SSI (Sky Status Indicator) is intended as a tool to detect the sky propagation status along a satellite path using ground-based brightness temperature values observed by a multi-channel microwave radiometer. In previous works, the authors reported boundary threshold values associated with three possible atmospheric propagation conditions: clear, cloudy and rainy sky. In this paper, focus was given to: a) the dependence on the site climatic characteristics of both coefficients involved in the SSI computation and SSI values themselves under non rainy conditions; b) the identification of possible uncertainties on the SSI capability due to radiometric resolution, improper calibration (bias), and elevation angle; c) the reliability of the SSI boundary threshold value between clear sky and cloudy conditions. The SSI features were investigated through an extensive simulation of radiometric parameters performed applying the Microwave Propagation Model for five elevation angle between 27.6 and 90°. In the simulation procedure, a proper cloud model was applied to the radiosonde profiles to calculate brightness temperatures in cloudy conditions. As the forward model does not yet include the contribution due to rainy scenarios, the analysis was limited to SSI values computed under clear and cloudy sky conditions.

As a general conclusion, and limited to the values that stem from simulations under clear sky conditions, a linear trend with the air mass is confirmed for the coefficient c_0, and to a lesser extent for the SSI and the boundary threshold value between clear and cloudy sky conditions, SSI_{CC}. This threshold was set equal to the SSI value at which the PDF of clear and cloudy sky conditions equal.

The climatic region (latitude) seems to have a certain impact as the numerical results computed for Milano (I) and Roma (I) show similarity and both differ from those computed for De Bilt (NL).

Furthermore, a robustness analysis of the boundary threshold value SSI_{CC} to measurement accuracy and improper instrument calibration was considered. To do this, the simulated $T_b(f)$ values were corrupted with AWGN with standard deviation equal to 0.25 K to account for the radiometric resolution. The SSI_{CC} showed variations of about 1 % of its noise free value. Besides, a bias of ±1 and ±4 K was added to reproduce measurements under improper calibration periods. The average SSI_{CC} computed from noisy brightness temperatures showed a sensitivity ranging from ± 2 % to -8/10 % in the best case and from about ±6 % to -18/+25 % in the worst case.

A numerical validation of the SSI_{CC} discrimination capabilities showed that a threshold-based criterion underestimates the number of cloudy condition occurrences of about 3 %, 5 % and 7 % in De Bilt, Milano and Roma, respectively. The underestimation is due to the fact the clear sky and cloudy conditions do not have a sharp separation as far as the SSI PDF is concerned. This fact derives from the physical processes in the atmosphere itself.

An analysis of the SSI_{CC} discrimination performances based on the Neyman-Pearson optimal detector can help experimenters in setting the boundary values according to the accepted rate of failure in the classification process.

Acknowledgement

The authors would like to thank the Royal Netherlands Meteorological Institute (KNMI) for providing the radiosonde profiles. Also, the authors are grateful to the referees for their helpful comments.

References

Basili P., Bonafoni S., Ciotti P., Pierdicca N. (2014) - *Modeling and sensing the vertical structure of the atmospheric path delay by microwave radiometry to correct SAR interferograms*. IEEE Transactions on Geoscience and Remote Sensing, 52 (2): 1324-1335. doi: http://dx.doi.org/10.1109/TGRS.2013.2250292.

Bosisio A.V., Capsoni C. (1995) - *Effectiveness of brightness temperature ratios as indicators of atmospheric path conditions*. Microwave Radiometry and Remote Sensing of Environment (Editor: D. Solimini), Utrecht (NL), pp. 129-138. ISBN 90-6764-189-8,VSP.

Bosisio A.V., Fionda E., Basili P., Carlesimo G., Martellucci A. (2012) - *Identification of rainy periods from ground-based microwave radiometry*. European Journal of Remote Sensing, 45: 41-50. doi: http://dx.doi.org/10.5721/EuJRS20124505.

Bosisio A.V., Ciotti P., Fionda E., Martellucci A. (2013a) - *Preliminary Results on the Performance of an Indicator to Identify the Status of the Sky Along a Satellite Link by Means of Ground-Based Brightness Temperatures*. Proceedings of 7th EUCAP, European Conference on Antenna and Propagation, Goteborg (SW), pp. 268-272.

Bosisio A.V., Fionda E., Ciotti P., Martellucci A. (2013b) - *A sky status indicator to detect rain-affected atmospheric thermal emissions observed at ground.* IEEE Transactions on Geoscience and Remote Sensing 51 (9): 4643-4649. doi: http://dx.doi.org/10.1109/TGRS.2013.2272589.

Bosisio A.V., Fionda E., Mattioli V., Ciotti P., Marzano F.S., Martellucci A. (2014) - *Accuracy of Real-time Sky Status Indicator (SSI) for the Characterization of a Satellite Communication Link At Microwave Bands*. Proceedings of 8th EUCAP, European Conference on Antenna and Propagation, The Hague (NL), pp. 268-272.

Crewell S., Löhnert U., Nörenberg D., Rose T., Martellucci A. (2009) - *Development of Ground Equipment for Atmospheric Propagation Assessment from 10 up to 90 GHz*. Proceedings of 3rd European Conference on Antennas and Propagation, EUCAP 2009, Berlin (D), pp. 2002-2006.

De Montera L., Barthès L., Mallet C., Golé P., Marsault T. (2010) - *Assessment of rain fade mitigation techniques in the EHF band on a Syracuse 3 20/44-GHz low elevation link*. Comptes Rendus Physique,11 (1):18-29. doi: http://dx.doi.org/10.1016/j.crhy.2009.12.002.

Elgered G., Rönnäng B.O., Askne J.I.H. (1982) - *Measurements of atmospheric water vapor with microwave radiometry*. Radio Science, 17 (5): 1258-1264. doi: http://dx.doi.org/10.1029/RS017i005p01258.

Fionda E., Basili P., Bonafoni S., Mattoli V., Ciotti P., Martellucci A. (2008) - *Retrieval algorithms of atmospheric parameters using thermal emission observed by surface based microwave operated in Cabauw*. ESA workshop on Radiowave Propagation 2008, Noordwijk (NL) December 3-5.

Gataullin Y. (2009) - *Real-time Fade Mitigation using radiometric measurements for future Ka-band services at DLR*. Proceedings of the 15th Ka-band and Broadband Communications, Navigation and Earth Observation Conference, Cagliari, Italy.

Hogg D.C., Guiraud F.O., Snider J.B., Decker M.T., Westwater E.R. (1983) -*A steerable dual-channel microwave radiometer for measurement of water vapor and liquid in the troposphere.* Journal of Climate and Applied Meteorology, 22: 789-806. doi: http://dx.doi.org/10.1175/1520-0450(1983)022<0789:ASDCMR>2.0.CO;2.

Keihm S.J., Marsh K.A. (1996) - *Advanced Algorithm and System Development for Cassini Radio Science Tropospheric Calibration*. The Telecommunications and Data Acquisition Progress Repor. 42-127, Jet Propulsion Laboratory, pp. 1-20.

Liebe H.J., Hufford G.A., Manabe T. (1991) - *A model for the complex permittivity of water at frequencies below 1 THz*. International Journal of Infrared and Millimeter Waves, 12 (7): 659-675. doi: http://dx.doi.org/10.1007/BF01008897.

Marzano F.S., Salemme P., Restuccia E., Consalvi F. (2012) - *Design and Characterization of the Q-band AlphaSat Receiving Station in Rome*. Proceedings of 6th European Conference on Antennas and Propagation (EUCAP), Prague, pp. 1468-1472. doi: http://dx.doi.org/10.1109/EuCAP.2012.6205993.

Mattioli V., Basili P., Bonafoni S., Ciotti P., Westwater E.R. (2009) - *Analysis and improvements of cloud models for propagation studies*. Radio Science, 44 (2): 1-13, doi: http://dx.doi.org/10.1029/2008RS003876.

Neyman J., Pearson K. (1933) - *On the problem of the most efficient test of statistical hypotheses*. Philosophical Transactions of the Royal Society of London, A (231): 492-510.

OPEX (1994) - *Reference book on Radiometry and Meteorological Measurements*. Second Workshop of Olympus Propagation Experimenters, 3 (8-10) November Noordwijk (NL), ESA WPP-083,1994.

Rose Th. (2008) - *ESA ATPROP System User's Manual*. Version 2.00, Radiometer Physics GmbH, available at: www.radiometer-physics.com.

Rosenkranz P.W. (1999) - *Correction to "Water Vapor Microwave Continuum Absorption: A Comparison Of Measurements And Models"*. Radio Science, 34 (4): 1025. doi: http://dx.doi.org/10.1029/1999RS900020.

Ruggieri M., Riva C., De Sanctis M., Rossi T. (2012) - *Alphasat TDP#5 Mission: Towards Future EHF Satellite Communications*. Proceedings of IEEE First AESS European Conference on Satellite Telecommunications (ESTEL), Rome, pp. 1-6, doi: http://dx.doi.org/10.1109/ESTEL.2012.6400076.

Salonen E., Uppala W. (1991) - *New prediction method of cloud attenuation*. Electronic Letters, 27 (12): 1106-1108. doi: http://dx.doi.org/10.1049/el:19910687.

Tanner A.B., Riley A.L. (2003) - *Design and performance of a high-stability water vapor radiometer*. Radio Science, 38 (3): 8050. doi: http://dx.doi.org/10.1029/2002RS002673.

Ware R., Carpenter R., Guldner J., Liljegren J., Nehrkorn T., Solheim F., Vandenberghe F. (2003) - *A multichannel radiometric profiler of temperature, humidity, and cloud liquid*. Radio Science, 38 (4): 8079. doi: http://dx.doi.org/10.1029/2002RS002856.

Westwater E.R. (1978) - *The Accuracy of Water Vapor and Cloud Liquid Determinations by Dual-Frequency Ground-Based Microwave Radiometry*. Radio Science, 13 (4): 677-685. doi: http://dx.doi.org/10.1029/RS013i004p00677.

Westwater E.R., Snider J.B., Falls M.J. (1990) - *Ground-based radiometric observations of atmospheric emission and attenuation at 20.6, 31.65, and 90 GHz: A comparison of measurements and theory*. IEEE Transactions on Antennas and Propagations, 38 (10): 1569-1579. doi: http://dx.doi.org/10.1109/8.59770.